J. Fluid Mech. (1980), *vol.* 99, *part* 2, *pp.* 267–292
Printed in Great Britain

A quasi-linear theory for rotating flow over topography. Part 1. Steady β-plane channel

By MICHAEL K. DAVEY

The Joint Institute for the Study of the Atmosphere and Ocean,
University of Washington, Seattle, Washington 98195, U.S.A.

(Received 8 May 1979 and in revised form 28 November 1979)

Steady rotating flow over topography in a periodic channel is examined, with emphasis on the interaction of waves, topography and mean flow. A simple quasi-linear theory is presented that features an implicit equation relating the net zonal flow to the forcing and topography. A good description of the dynamics is obtained, even when resonant Rossby waves appear. Multiple solutions for given external parameters are predicted in some cases, and confirmed by comparison with a fully nonlinear numerical model.

The nonlinear results also indicate that the zonally averaged shear can be important when topographic effects or Rossby numbers are large. With this factor taken into account the theory gives good agreement with the fully nonlinear model, as long as eddy–eddy interactions are minor.

The theory is relevant to the dynamics of planetary waves in the atmosphere, and may also be applied to some oceanic problems.

1. Introduction

The large-scale ($O(1000$ km)) currents in the ocean and atmosphere are almost horizontal and non-divergent. However, their courses are strongly influenced by the small vertical motion caused by mountains, heat sources, and frictionally induced divergence at boundaries. Some of the first analyses of such effects on the atmosphere have been given by Charney & Eliassen (1949) and Smagorinsky (1953). Further work using detailed numerical models, in conjuction with analysis of observations, has helped identify the important role of these effects (see, for example, Manabe & Terpstra 1974). Recently Grose & Hoskins (1979) have used a barotropic model with realistic topography and mean zonal flow to calculate flow patterns in good agreement with seasonally averaged upper-troposphere observations.

The aim of the work presented here is to develop a simple theory to describe the effect of obstacles on large-scale rotating flow in recycling systems, with eventual application to the atmosphere and ocean in mind. In part 1 flow in a periodic channel is analysed to describe the dynamics simply. More complicated annular geometry is treated in part 2. (The annulus case includes the additional effect of meridional vorticity advection on the net zonal flow. It is also more suitable for comparison with laboratory experiments.)

Steady flow in an annulus has been previously described by Davey (1978), and the present theory is an extension and improvement of Davey's to include the β-effect and associated Rossby-wave dynamics. Unlike other related papers on waves generated

0022-1120/80/4484-1490 $02.00

by topography (e.g. Neumann 1960; Clarke & Fofonoff 1969; McCartney 1976) the strength of the basic zonal flow is not prescribed but is allowed to adjust to the interaction of waves and topography. Feedback then occurs that can make the system very sensitive to small changes in the forcing, particularly when Rossby waves are present and dissipation is weak. (This is the situation in the atmosphere on a planetary scale, and it may also apply to the ocean circulation.) For such systems standard perturbation methods of analysis can give unsatisfactory results due to the neglect of changes in the basic flow. The quasi-linear theory described in the following sections pays proper attention to such effects.

The sensitivity to the forcing may be relevant to blocking in the atmosphere, whereby a particular flow pattern can appear and persist for an unusually long time. (Egger 1978 gives an account of such events, together with some numerical simulations.) Recent studies with this application have been made by Charney & DeVore (1979) and Hart (1979), with emphasis on the occurrence of multiple equilibria for given external parameters. (Charney & DeVore examine transitions between alternative states, and Hart discusses changes due to variations in external forcing.) The phenomenon of multiple steady states is also predicted by this quasi-linear theory. As part of this paper the dynamics of alternative blocked and unblocked states are described, and the effect of nonlinear interactions on their occurrence is discussed.

The general theory for quasi-geostrophic barotropic flow in a β-plane channel is given in §2. (Time dependence is included in anticipation of a later analysis of the transition from steady to oscillatory solutions.) The system is forced, via Ekman layers, by a prescribed surface velocity. A surface wind stress can be substituted for oceanic applications. (For the atmosphere a meridional temperature gradient should be used and the upper Ekman layer removed, but the internal dynamics is fundamentally unchanged.) For the simplest quasi-linear approximation described in §3 most nonlinear interactions are discarded; only the zonal average of eddy–topography interaction is retained to allow mean flow changes. An implicit equation relating net zonal flow to forcing and topography can then be obtained.

In §4 results from this theory are given for flow over a simple obstacle. The effects of varying forcing and dissipation are shown, and multiple solutions with and without the β-effect are discussed. Simple dynamical explanations are offered for the features seen.

To check the theory a nonlinear numerical model was developed. Results from the two models are compared in §5, and good agreement is found at low Rossby number, including verification of multiple solutions. For larger Rossby numbers (stronger forcing) the results differ owing to the neglect of mean shear. An improved theory is described in §6, and some limitations on multiple solution regimes are obtained. Finally the results are summarized in §7, with a discussion of applications.

2. Basic equations

The geometry for the rotating channel is shown in figure 1. The channel has periodic length $2\pi L$, width bL, and average depth H_0. The y axis should be regarded as the northward direction, the x axis eastward. A horizontal velocity $\mathbf{u}_r^*$ is prescribed at the upper surface $z^* = H_0$ to drive the flow. The topography $z^* = h^*(x, y)$ has height

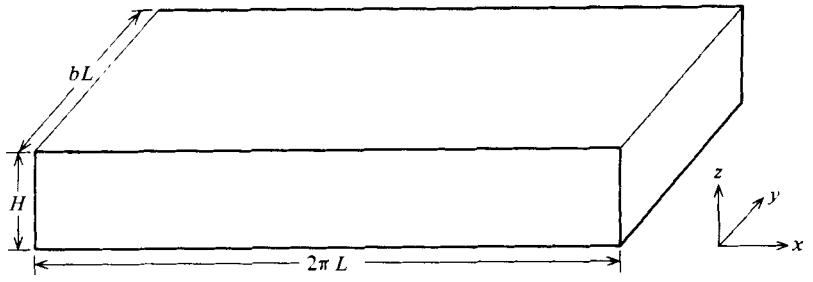

FIGURE 1. Geometry for the periodic channel, with side walls at $y = 0, bL$.

scale $h_0^* \ll H_0$. Variation of rotation rate with latitude is simulated by using a β-plane, so the Coriolis parameter is

$$f = f_0 + \beta^*(y^* - \tfrac{1}{2}bL),$$

where $\frac{1}{2}f_0$ is the mid-channel rotation rate.

For motion with a time scale much greater than $1/f_0$, as assumed here, the bulk of the flow is quasi-geostrophic. This interior flow is driven and dissipated via thin Ekman layers at the upper and lower boundaries. Stratification effects are neglected, so only the barotropic (depth-averaged) component is considered. The vertical component of vorticity for this flow is changed relative to its basic value f_0 by changes in f and by stretching of vertical fluid columns by topographic variations and Ekman-layer divergence. These effects thus determine the course of the flow. (A more detailed account of the dynamics may be found in Pedlosky 1971.)

Some non-dimensional variables are defined as follows (asterisks denote dimensional variables):

$$(u^*, v^*) = C(u, v), \quad w^* = C(H_0/L)\, w,$$

$$(x^*, y^*) = L(x, y), \quad z^* = H_0 z,$$

$$p^* = Cf_0 Lp, \quad t^* = t/\omega f_0.$$

The pressure when the system is at rest has been removed from the hydrostatic pressure p; C is a horizontal velocity scale; and ω is a non-dimensional time scale. Important non-dimensional parameters are the Rossby number

$$\epsilon = C/f_0 L$$

and the Ekman number $$E = 2\nu/f_0 H_0^2.$$

(ν is an eddy viscosity.)

We also define β-effect and topography-height parameters by

$$\beta = \beta^* L/f_0, \quad h_0 = h_0^*/H_0.$$

It is assumed that ϵ, $E^{\frac{1}{2}}$, β and h_0 are all small compared to unity, as is appropriate for large-scale geophysical flow over shallow obstacles.

To lowest order the interior flow is in geostrophic balance, so

$$v = p_x, \quad u = -p_y, \tag{2.1}$$

and $p(x, y)$ is a stream function for $\mathbf{u}(x, y)$. The control of this flow by small vertical motions is described by the quasi-geostrophic vorticity equation

$$\omega\zeta_t + \epsilon\mathbf{u}.\nabla\zeta + \beta v = w_z$$
$$= \tfrac{1}{2}E^{\frac{1}{2}}\zeta_T - E^{\frac{1}{2}}\zeta - \mathbf{u}.\nabla h, \tag{2.2}$$

where ζ and ζ_T are the interior and prescribed upper surface vorticities. In terms of p, (2.1) can be written as

$$\omega\nabla^2 p_t + J(p, \epsilon\nabla^2 p + \beta y + h) + E^{\frac{1}{2}}\nabla^2 p = \tfrac{1}{2}E^{\frac{1}{2}}\zeta_T, \tag{2.3}$$

where the Jacobian operator J is defined by

$$J(p, q) = p_x q_y - p_y q_x.$$

Periodicity of the system requires

$$p(-\pi, y, t) = p(\pi, y, t). \tag{2.4}$$

The side walls are streamlines, so boundary conditions are

$$p(x, 0, t) = 0, \quad p(x, b, t) = -Q(t). \tag{2.5}$$

The spatial constant Q can be expressed as

$$Q = \int_0^b u\,dy = Ub, \tag{2.6}$$

where U is the average velocity in the channel. To $O(1)$ the channel depth is unity, so Q is also the lowest-order estimate of the net zonal transport in the channel.

At this stage Q is not determined so an extra constraint is needed to close the problem mathematically. By balancing interior and Ekman-layer transports to $O(E^{\frac{1}{2}})$ we obtain the time-dependent version of the circulation condition used in Davey (1978). This is

$$\oint \{\omega\mathbf{u}_t + E^{\frac{1}{2}}\mathbf{u} - \tfrac{1}{2}E^{\frac{1}{2}}\mathbf{u}_T\}.\mathbf{dl} = 0, \tag{2.7}$$

where the integral is taken around any streamline at time t. In particular, on the side walls $y = 0, b$ (2.7) leads to

$$\left(\omega\frac{d}{dt} + E^{\frac{1}{2}}\right)\int_{-\pi}^{\pi} u\,dx = \tfrac{1}{2}E^{\frac{1}{2}}\int_{-\pi}^{\pi} u_T\,dx. \tag{2.8}$$

This condition is necessary and sufficient to determine p.

For convenience and simplicity we now restrict attention to the uniform surface flow

$$\mathbf{u}_T = (2U_0, 0). \tag{2.9}$$

($U_0 = \pm 1$ will be used to investigate eastward and westward flow.) Further, only topography that has zero zonal average and vanishes on side walls will be considered. We put

$$p = -U(t)\,y + \Phi(y, t) + \phi(x, y, t), \tag{2.10}$$

where Φ represents zonally averaged shear and ϕ corresponds to the remaining eddies (waves). The boundary condition (2.5) requires

$$\Phi = \phi = 0, \quad y = 0, b. \tag{2.11}$$

Taking the zonal average of (2.3) leads to

$$\left(\omega\frac{\partial}{\partial t}+E^{\frac{1}{2}}\right)\Phi_{yy}+[J(\phi,\epsilon\nabla^2\phi+h)]=0 \tag{2.12a}$$

(a zonal average will be indicated by square brackets). This leaves

$$\omega\nabla^2\phi_t+[u](\epsilon\nabla^2\phi+h)_x+\beta\phi_x+E^{\frac{1}{2}}\nabla^2\phi+J(\phi,\epsilon\nabla^2\phi+h)-[J(\phi,\epsilon\nabla^2\phi+h)]=0. \tag{2.12b}$$

With an integration by parts the zonal-average term in (2.12) becomes

$$\begin{aligned}[J(\phi,\epsilon\nabla^2\phi+h)] &= -[\phi(\epsilon\nabla^2\phi+h)_{xy}+\phi_y(\epsilon\nabla^2\phi+h)_x]\\ &= -\frac{\partial}{\partial y}[\phi(\epsilon\nabla^2\phi+h)_x].\end{aligned} \tag{2.13}$$

From the side-wall circulation condition (2.8) we have

$$\left(\omega\frac{\partial}{\partial t}+E^{\frac{1}{2}}\right)[u]=E^{\frac{1}{2}}U_0,\quad y=0,b. \tag{2.14}$$

Integrating (2.12a) from 0 to y using (2.13) and (2.14) then leads to

$$\left(\omega\frac{\partial}{\partial t}+E^{\frac{1}{2}}\right)[u]=E^{\frac{1}{2}}U_0-[\phi(\epsilon\nabla^2\phi+h)_x]. \tag{2.15}$$

Integrating again across the channel gives

$$\left(\omega\frac{d}{dt}+E^{\frac{1}{2}}\right)Ub=E^{\frac{1}{2}}U_0\,b-\frac{1}{2\pi}\int_0^b\int_{-\pi}^{\pi}\phi(\epsilon\nabla^2\phi+h)_x\,dx\,dy. \tag{2.16}$$

The double integral of $\phi\nabla^2\phi_x$ vanishes (using (2.11) and periodicity), so the required equation for Q is

$$\omega Q_t+E^{\frac{1}{2}}Q=E^{\frac{1}{2}}Q_0-\frac{1}{2\pi}\int\int\phi h_x\,dx\,dy,$$

where $Q_0=U_0\,b$.

A useful alternative form of this equation that relates Q to the total kinetic energy is derived in appendix A. One use is that for a steady state (A 5) gives

$$b(U_0-U)=\frac{1}{2\pi U}\int\int\Phi_y^2+\phi_x^2+\phi_y^2\,dx\,dy. \tag{2.17}$$

The integral is positive or zero, so in equilibrium we have

$$0<U/U_0\leqslant 1. \tag{2.18}$$

3. The simplest steady quasi-linear theory

When the topography is flat the steady response to $\mathbf{u}_T=(2U_0,0)$ is simply

$$\mathbf{u}=(U_0,0). \tag{3.1}$$

In general, however, the system is nonlinear and has not been solved exactly. The standard technique for obtaining approximate solutions is to consider small perturbations to (3.1) and linearize the equations. It was found that this method (outlined in

appendix B) gives poor results when the β-effect is included, unless the perturbations are uninterestingly small. This failure can be remedied by allowing the mean flow to adjust to topographic effects.

For the simplest quasi-linear theory all but the zonal averages of interactions between eddies, mean shear and topography are discarded. (This assumption of weak nonlinearity will be tested in §5 by comparing results with fully nonlinear numerical solutions.) Effectively advection of $\epsilon\zeta+h$ by eddies and mean shear is removed and (2.12b) reduces to

$$\epsilon U\nabla^2\phi_x+\beta\phi_x+E^{\frac{1}{2}}\nabla^2\phi+Uh_x=0. \tag{3.2}$$

The term Uh_x represents generation of eddy vorticity by the zonal mean flow over the topography. This must be balanced by zonal advection by U, meridional advection of background vorticity βy, and dissipation. The essential difference between (3.2) and linear methods is that U is not prescribed.

The transport equation (2.16) gives for a steady state

$$b(U_0-U)=\frac{1}{2\pi E^{\frac{1}{2}}}\int\int\phi h_x\,dx\,dy. \tag{3.3}$$

The term on the right will be referred to as the topographic drag. An alternative expression is, from (3.2),

$$\frac{1}{2\pi E^{\frac{1}{2}}}\int\int\phi h_x\,dx\,dy=\frac{1}{U}\int\int(\phi_x^2+\phi_y^2)\,dx\,dy. \tag{3.4}$$

(The mean shear contribution in the exact version (2.17) does not appear in (3.4) due to the neglect of eddy–shear interactions in (3.2).)

With boundary conditions (2.11), (3.2) can be solved to find ϕ in terms of U. Equation (3.3) then becomes an implicit equation for U as a function of the forcing and topography. It is apparent that for this theory the mean shear (which can be found from (2.15)) does not influence U and ϕ, but serves only to match the side-wall circulation conditions.

As an example we consider the topography

$$h=h_0H(y)\sum_{m=1}^{M}F_m\cos mx, \tag{3.5}$$

and in particular choose the meridional profile

$$H(y)=\sin ly \tag{3.6}$$

with $l=n\pi/b$, and integers m, n. The perturbation ϕ then takes the form

$$\phi=\sin ly\sum_{1}^{M}A_m\cos mx+B_m\sin mx. \tag{3.7}$$

(Note that $[\phi\nabla^2\phi_x]=0$ for this simple example.)

From (3.2) and (3.7) we find

$$A_m=-Uh_0mF_m m(\beta-\epsilon UK^2)/D_m, \tag{3.8a}$$

$$B_m=-Uh_0mF_mE^{\frac{1}{2}}K^2/D_m, \tag{3.8b}$$

where $$D_m=EK^4+m^2(\beta-\epsilon UK^2)^2,\quad K^2=m^2+l^2.$$

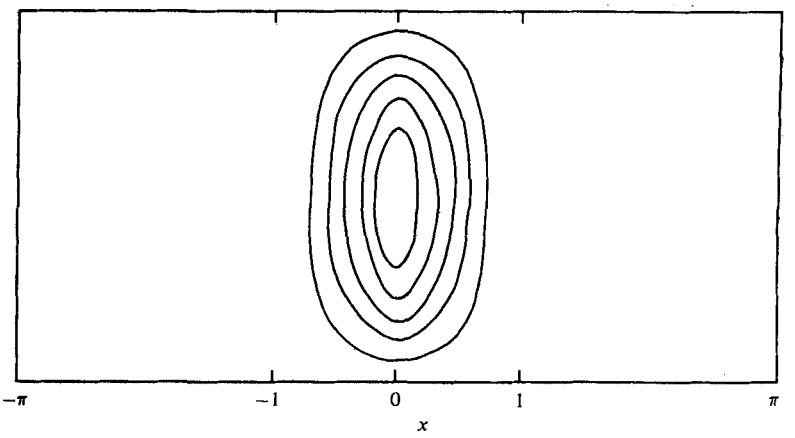

FIGURE 2. Contours of the topography with triangular x profile, as approximated by truncated Fourier series.

The transport equation (3.3) gives, with some rearrangement,

$$\frac{U}{U_0} = 1 - \tfrac{1}{4}h_0^2 \frac{U}{U_0} \sum_1^M m^2 F_m^2 K^2 \Big/ (EK^4 + m^2(\beta - \epsilon U K^2)^2). \tag{3.9}$$

(This is a polynomial in U of degree $2M+1$.)
From (2.15) the mean flow can be calculated using (3.8) and (3.9), giving

$$[u] = U_0 - 2(U_0 - U)\sin^2 ly. \tag{3.10}$$

An important feature of (3.9) is that there may be several solutions for any one set of external parameters. However there is a unique U, and ϵ, corresponding to each internal Rossby number ϵU. This is apparent from the rearrangement of (3.9) as

$$\frac{U}{U_0} = \{1 + \tfrac{1}{4}h_0^2 \Sigma m^2 F_m^2 K^2 / D_m\}^{-1}. \tag{3.11}$$

Similarly there may be multiple solutions for U for any one topography height, but there is only one $h_0 > 0$ for each U.

4. Results from the simplest quasi-linear theory

To illustrate the theory described in the previous section results for a particular system will be described. An obstacle is chosen with a triangular x profile of half-width $x_0 = 1$, and $\sin y$ cross-channel dependence. Contours of this topography are shown in figure 2. (The first ten terms of the Fourier representation (3.5) were used.) The channel width is $b = \pi$.

Streamlines (contours of $-Uy + \Phi + \phi$) are given in figure 3, for $\beta = 0{\cdot}2$, $E^{\frac{1}{2}} = 0{\cdot}02$, $h_0 = 0{\cdot}2$ and various ϵ. These show the effect of varying the forcing when dissipation is small. For westward flow (figure 3*a*) the topographic effect is small and U is little changed from U_0. With eastward forcing of the same magnitude the disturbance is much larger and U is almost halved (see figure 3*b*). A wave pattern occurs downstream of the obstacle, as expected for eastward flow on a β-plane. Note that this wave decays only slowly downstream and hence affects the flow pattern upstream of the obstacle. For

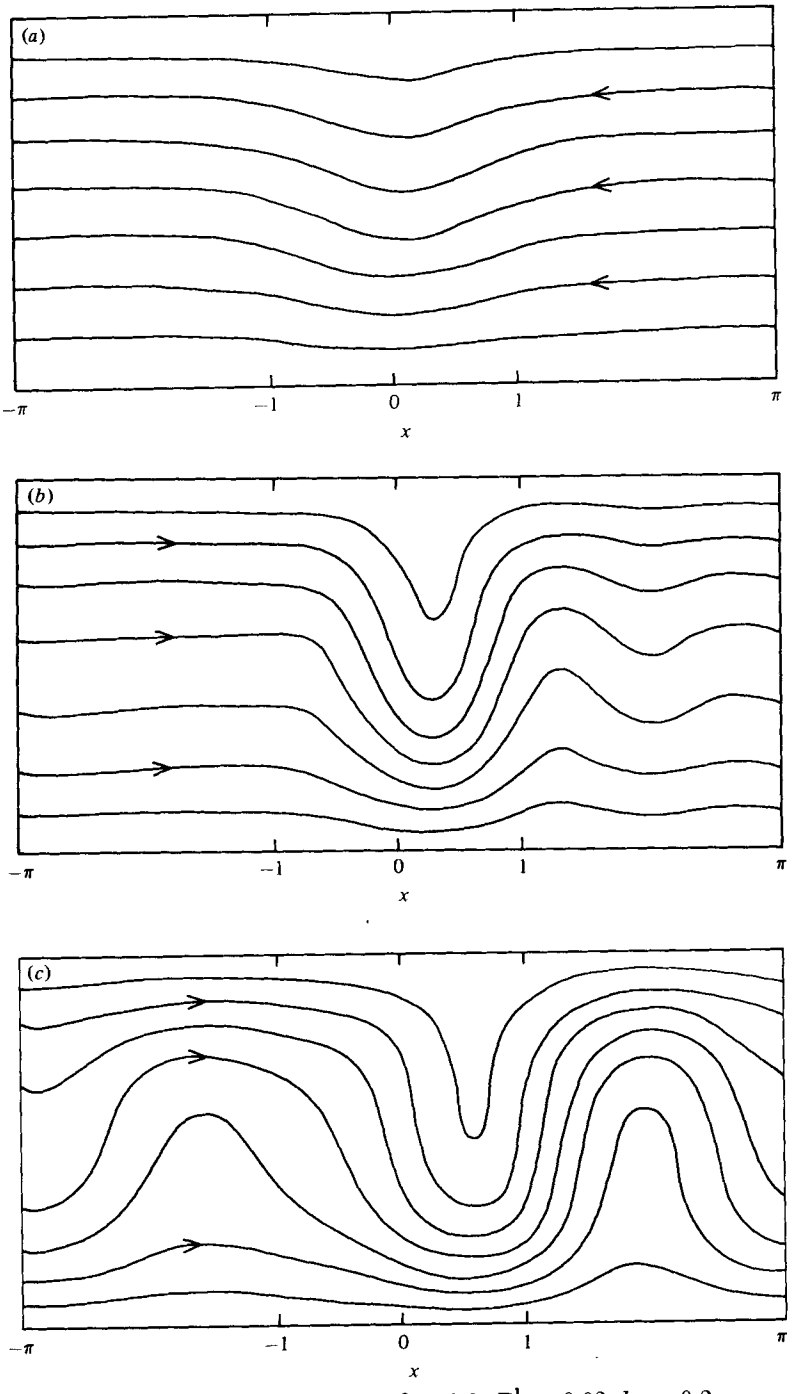

FIGURE 3. Streamlines for $\beta = 0{\cdot}2$, $E^{\frac{1}{2}} = 0{\cdot}02$, $h = 0{\cdot}2$.

(*a*) $U_0 = -1$, $\epsilon = 0{\cdot}05$, $U = -0{\cdot}97$.

(*b*) $U_0 = 1$, $\epsilon = 0{\cdot}05$, $U = 0{\cdot}58$.

(*c*) $U_0 = 1$, $\epsilon = 0{\cdot}014$, $U = 0{\cdot}72$.

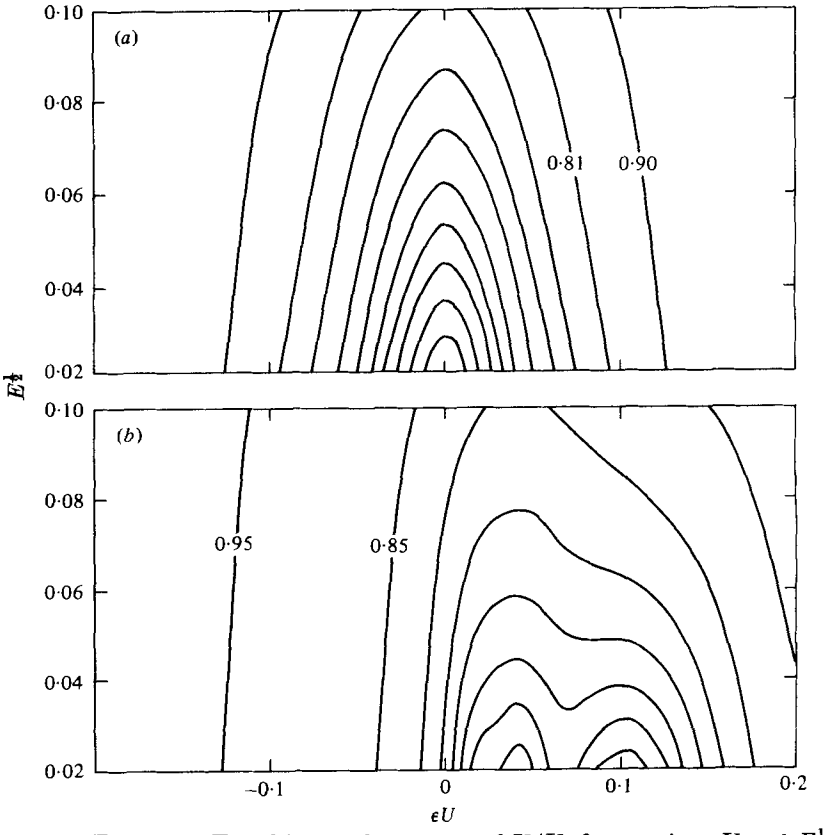

FIGURE 4. Equal-interval contours of U/U_0 for varying ϵU and $E^{\frac{1}{2}}$, with $h_0 = 0{\cdot}4$. (*a*) $\beta = 0$, (*b*) $\beta = 0{\cdot}2$.

weaker forcing the wavelength is smaller and the disturbance decays more rapidly, as can be seen by comparing figures 3(*b*, *c*).

The net zonal flow magnitude U/U_0 is shown in figure 4 as a function of $E^{\frac{1}{2}}$ and ϵU, calculated using equation (3.11); ϵU is used rather than ϵ because U/U_0 is a single-valued function of ϵU, but may be a multiple-valued function of ϵ. When $\beta = 0$ there is a steady increase in U/U_0 as $|\epsilon U|$ or $E^{\frac{1}{2}}$ increases, and the result is the same for eastward and westward flow (figure 4*a*). By contrast, when $\beta > 0$ (figure 4*b*) the result is not symmetric and a series of minima appear for eastward flow ($\epsilon U > 0$). For given $E^{\frac{1}{2}}$ these minima occur at $\epsilon U \approx \beta/K^2$, and are most prominent for small $E^{\frac{1}{2}}$. (They broaden and fade with increasing dissipation.) For westward flow there are no minima. The behaviour for $\epsilon U < 0$ is like that when $\beta = 0$, with U/U_0 increased a little. The same general features are found for different topography heights, but the relative magnitudes of the minima depend on the topography shape. (Higher wavenumbers are emphasized for narrower obstacles.)

The behaviour described above is best explained by first considering one topographic mode, $\cos mx \sin ly$ say. The zonal flow U over this topography produces vorticity $\nabla^2\phi$ of the same pattern, with some phase shift. This pattern is advected downstream by U. In addition induced lateral movement causes further vorticity changes via the

β-effect, such that the wave propagates at a speed $-\beta/\epsilon K^2$. This Rossby wave propagation is equivalent to zonal advection, as can be seen from the identity

$$\beta v = \beta\phi_x = -(\beta/K^2)\nabla^2\phi_x$$

for sinusoidal disturbance ϕ. The net effect is that the wave is 'advected' at a speed U_R relative to the topography, with

$$\epsilon U_R = \epsilon U - \beta/K^2. \tag{4.1}$$

For this single mode (3.2) gives

$$\epsilon U_R \nabla^2\phi_x + E^{\frac{1}{2}}\nabla^2\phi + Uh_x = 0, \tag{4.2}$$

which expresses the balance of vorticity 'advection', dissipation and generation.

When $|\epsilon U_R| \gg E^{\frac{1}{2}}$ the main balance is between 'advection' and generation. The eddy stream function ϕ is then almost in phase with the topography and the topographic drag is correspondingly low, according to (3.3). As $|\epsilon U_R|$ decreases a larger perturbation is needed to balance Uh_x, and topographic drag increases accordingly. (Note that the need for larger $\nabla^2\phi$ is offset somewhat by the decrease in $|U|$. The change in U also affects U_R.)

With $|\epsilon U_R| \lesssim E^{\frac{1}{2}}$ dissipation becomes important. Then h and ϕ become more out of phase and U/U_0 is further decreased. The minimum occurs when $\epsilon U \to \beta/K^2$, when large eddies and low U are required for a balance of dissipation and generation. In this case, when $\beta \neq 0$, a resonant standing Rossby wave occurs with its amplitude limited only by dissipation, according to this theory.

When several modes are present the situation is changed somewhat because the separate responses cannot be superimposed. When $\beta \neq 0$ each mode still has a distinct minimum, but its magnitude is reduced by the presence of other modes. The several minima seen in figure 4(*b*) are due to the excitation of standing Rossby waves of various wavenumbers. When $\beta = 0$ the minima all occur at the limit $\epsilon \to 0$.

The topographic effect diminishes as $|U_R|$ increases. Hence for westward flow U/U_0 is increased by increasing ϵ and by the β-effect. For eastward flow disturbances decrease when ϵ increases beyond the largest value of β/K^2.

It is interesting to note that U_R changes sign when ϵU passes a resonance point β/K^2. For small $E^{\frac{1}{2}}$ there is then a rapid phase reversal of ϕ, so a dramatic change in flow pattern can be caused by a small change in ϵU.

The system can evidently be very sensitive to the parameter ϵU. This internal Rossby number (based on the mean flow speed) depends on the effect of topography on U, via eddy–topography interactions. The quasi-linear theory is an improvement on the standard perturbation method because this dependence is included.

An important feature of the theory is the occurrence of multiple equilibria for fixed external parameters. When h_0 (or ϵ) is small there is only one solution to (3.9), but as h_0 (or ϵ) is increased there may be more than one solution for some ranges of ϵ (or h_0). This behaviour can be seen in figure 5, which shows the response of U/U_0 to varying ϵ with $\beta > 0$. (The topography used is that of figure 2.) The multiple solutions appear for eastward flow, and overlap more as h_0 increases. The minima in U/U_0 occur very close to resonance points β/K^2; the slight discrepancy is caused by having several modes in the system. (The curves $\epsilon U = \beta/K^2$ are given in figure 6 for a few wavenumbers.)

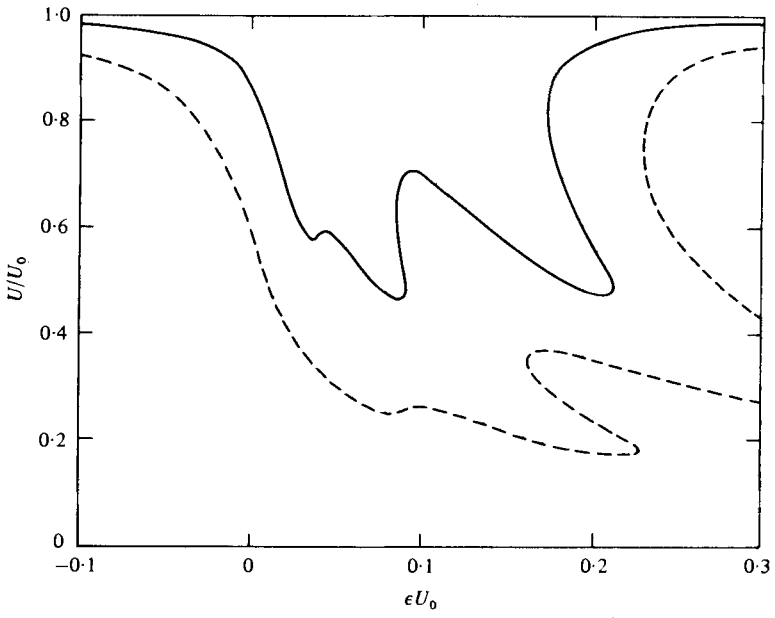

FIGURE 5. U/U_0 as a function of ϵU_0, with $\beta = 0{\cdot}2$, $E^{\frac{1}{2}} = 0{\cdot}02$, $h_0 = 0{\cdot}2$ (solid curve), $h_0 = 0{\cdot}4$ (dashed curve).

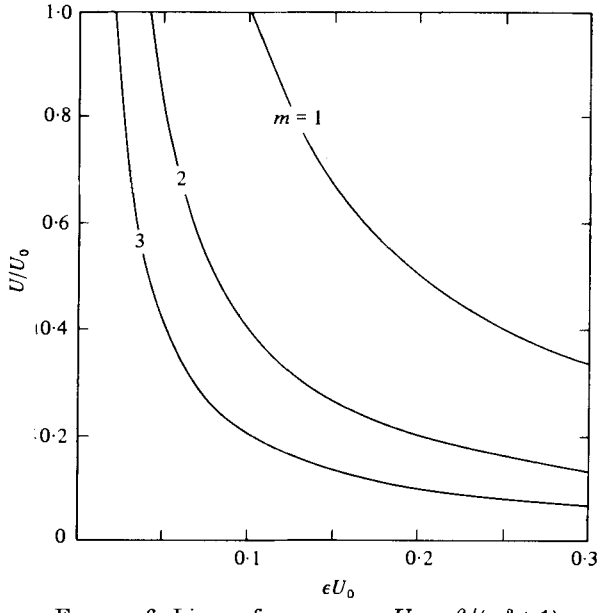

FIGURE 6. Lines of resonance $\epsilon U = \beta/(m^2+1)$.

The stability of the solutions was determined by using time-dependent linear analysis of small perturbations from equilibrium. It was found that single solutions are always stable. When three alternatives occur, however, the high-U and low-U solutions are stable, while the middle branch is unstable.

These stability properties can be largely explained by a simple argument. First

consider the portion of the equilibrium curve where $dU/d\epsilon < 0$ and $\epsilon U < \beta/K^2$. (The quantity K^2 corresponds to the dominant wave for that region.) A small increase in ϵ will decrease U_R. The topographic drag then increases and U decreases, so the system moves towards a new equilibrium point on the same branch. (The decrease in U also increases U_R again, thus providing a brake on the change in U.) Likewise such a point is stable for a small decrease in ϵ. A similar argument can be made for stability when $dU/d\epsilon > 0$ and $\epsilon U > \beta/K^2$. (This category includes a small region near a local minimum.) An increase in ϵ will increase U_R and in turn increase U, again towards equilibrium on the same branch. This further increases U_R. In this case the increase in U is retarded by increased vorticity generation Uh_x. (A jump from a lower to upper branch occurs when this mechanism cannot counteract the increase in U.) When $dU/d\epsilon < 0$ and $\epsilon U > \beta/K^2$, however, a change in ϵ causes a shift in U away from the middle branch toward an upper or lower branch.

Charney & DeVore (1979) and Hart (1979) have investigated multiple equilibria in similar situations. They also found that the central of three branches was unstable. Charney & DeVore, using single-mode topography and a severely truncated nonlinear model, found that the lower branch in their case could be unstable to higher-mode disturbances. Hart has considered finite-amplitude perturbations, and a discussion of limit cycles is included in his paper.

Another stability property is worth mentioning. If ϵU is fixed (and ϵ is allowed to vary) then this quasi-linear theory becomes linear and all equilibrium solutions are stable. A time-dependent system can thus converge to an 'unstable' steady state with this constraint.

For multiple solutions with low U we find $\epsilon U \approx \beta/K^2$, so there is a balance of dissipation and generation as discussed earlier. (Such a solution, with large eddies and weak mean flow, is called a blocked system.) The alternative with larger U has $\epsilon U > \beta/K^2$ and there is a balance of advection and generation. Examples of blocked and unblocked flow patterns can be seen in figures 9 and 14. Note how one mode dominates these solutions, and is out of phase and in phase with the topography for the blocked and unblocked systems respectively.

The above discussion has concentrated on multiple equilibria with the β-effect. The simplest quasilinear theory also predicts multiple equilibria when $\beta = 0$. Calculations for this case were made using the simpler topography $h = h_0 \cos x \sin y$. Equation (3.9) then reduces to the cubic

$$\epsilon^2(U/U_0)^3 - \epsilon^2(U/U_0)^2 + (E + \tfrac{1}{8}h_0^2)\, U/U_0 - E = 0, \tag{4.3}$$

and reasonably simple conditions for multiplicity can be found. For example, a sufficient (but not necessary) condition for multiple equilibria is

$$4(E + \tfrac{1}{8}h_0^2) < \epsilon^2 < \tfrac{9}{2}(\tfrac{1}{8}h_0^2 - \tfrac{1}{2}E), \tag{4.4}$$

whereas a necessary but not sufficient condition is

$$3(E + \tfrac{1}{8}h_0^2) < \epsilon^2 < (E + \tfrac{1}{8}h_0^2)\,(19E + \tfrac{1}{8}h_0^2)/4E. \tag{4.5}$$

Graphs of U/U_0 as a function of ϵU_0 are given in figure 7. It is evident that very low U/U_0 is required for multiple solutions. (This is needed to get the alternative dissipation–generation and advection–generation balances.) It will be seen later that the theory is not valid for such large flow changes, and that more accurate calculations show no such multiplicity.

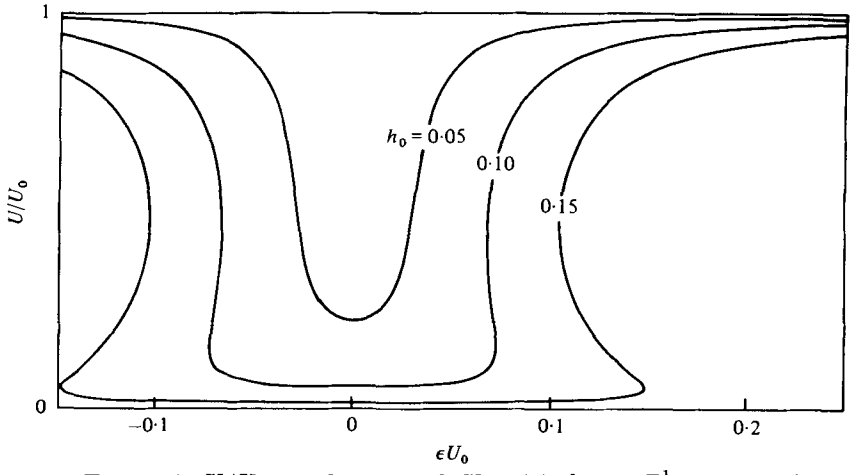

FIGURE 7. U/U_0 as a function of ϵU_0, with $\beta = 0$, $E^{\frac{1}{2}} = 0{\cdot}01$, using $\cos x \sin y$ topography with h_0 as indicated.

The simple quasi-linear theory predicts some interesting phenomena. In the next section these results are tested by comparison with those from a fully nonlinear numerical model.

5. Comparison with a fully nonlinear model

A spectrally truncated time-dependent numerical model was developed in conjunction with the quasi-linear theory. All nonlinear terms were retained, and equations for the spectral coefficients found from the vorticity and transport equations. (Details are given in appendix C.) Steady solutions were obtained by time-stepping from some initial conditions. The topography of figure 2 was again used, with $\beta = 0{\cdot}2$, $E^{\frac{1}{2}} = 0{\cdot}01$, $h_0 = 0{\cdot}075$. (These values are not intended to simulate any actual situation, but rather chosen to show contrasting results.)

The dependence of U on ϵ for the numerical and simple quasi-linear models is shown in figure 8. For relatively small values of ϵ (less than about 0·1 for this example) the positions of minima agree well, with the quasi-linear theory somewhat overestimating the topographic drag. In both cases multiple solutions are found near the $m = 2$ resonance point, though the region of overlapping branches is smaller than predicted.

Upper branch steady states were found using the initial flow $\mathbf{u} = (1, 0)$, whereas the lower branch was obtained with $\mathbf{u} = (0, 0)$ initially. To define further the multiple solution regime a steady state on one branch was reached, then ϵ was gradually changed. (It was thought that this would increase the chance of finding multiple solutions by closely following the alternative branches. In practice, however, no extra states were found that could not be reached from the uniform initial conditions.) The upper and lower branches overlapped for $0{\cdot}057 < \epsilon < 0{\cdot}060$. A change in ϵ of 0·0005 was sufficient to trigger a slow drift from one branch to the other. (Near resonance points long times were needed to reach a steady state, typically about ten spin-up times $O(\omega E^{-\frac{1}{2}})$. This sluggish behaviour is due to the slow group velocity of the dominant Rossby wave, as discussed by McIntyre (1968).)

Another method used to obtain steady solutions was to fix ϵU and to allow ϵ to

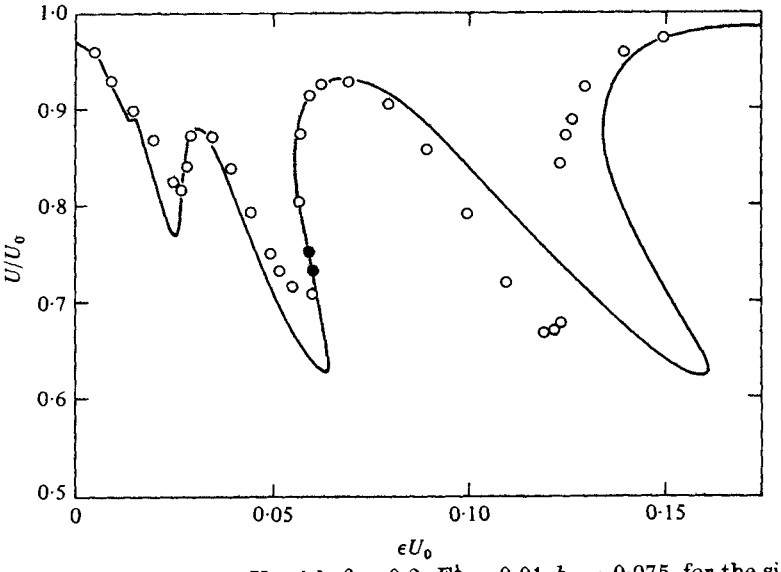

FIGURE 8. U/U_0 as a function of ϵU_0 with $\beta = 0{\cdot}2$, $E^{\frac{1}{2}} = 0{\cdot}01$, $h_0 = 0{\cdot}075$, for the simplest quasi-linear (solid line) and fully nonlinear (open circles) models. The solid circles indicate unstable fully nonlinear results.

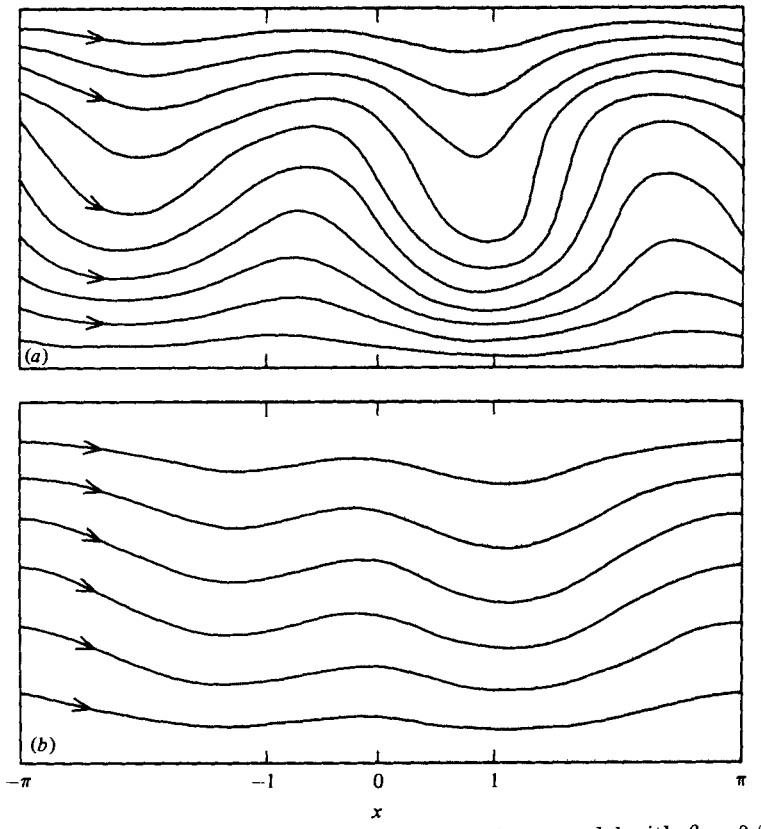

FIGURE 9. Alternative flow patterns from the fully nonlinear model with $\beta = 0{\cdot}2$, $E^{\frac{1}{2}} = 0{\cdot}01$, $h_0 = 0{\cdot}075$, $\epsilon = 0{\cdot}06$. (*a*) $U = 0{\cdot}71$, (*b*) $U = 0{\cdot}92$.

vary. (The mean flow U evolved according to the transport equation (2.16), and at each time-step ϵ was adjusted to keep ϵU constant.) In this way different branches could be reached from the same initial state $\mathbf{u} = (1, 0)$ by choosing different ϵU. The points shown as solid circles in figure 8 are unstable states found by this method. (When the constraint of constant ϵU was removed and ϵ fixed these solutions drifted very slowly towards one of the stable alternatives.) These points agree with the unstable branch predicted by the quasi-linear theory.

Figure 9 shows streamlines for the two stable numerical solutions found at $\epsilon = 0{\cdot}06$. The $(m, n) = (2, 1)$ wave is clearly dominant, as expected. The blocked mode (figure 9*a*) has $U = 0{\cdot}71$, whereas the other has $U = 0{\cdot}92$. The quasi-linear theory gives multiple solutions for the same parameters that are very similar to the numerical results.

For larger ϵ the numerical and simple quasi-linear results do not agree near the $m = 1$ resonance point. The difference is not obvious in the flow patterns, which are dominated by the $(m, n) = (1, 1)$ wave in each case, but is clearly seen in the variation of U with ϵ. In particular no multiple solutions were found in this region using the fully nonlinear model, in contrast to the quasi-linear prediction. (The system is still very sensitive to ϵ near the predicted resonance point, however.)

The discrepancy is mainly due to the omission of the zonally averaged shear. A modified theory that takes this into account is given in the next section.

6. An improved quasi-linear theory

When the zonally averaged shear is retained, but eddy–eddy interactions are still omitted, the steady eddy-vorticity equation is

$$\epsilon[u]\nabla^2\phi_x + (\beta - \epsilon[u]_{yy})\phi_x + E^{\frac{1}{2}}\nabla^2\phi + [u]h_x = 0. \tag{6.1}$$

In general we can use

$$\phi = \sum_m a_m(y)\cos mx + b_m(y)\sin mx. \tag{6.2}$$

Then with topography given by (3.5) the ordinary differential equations for the coefficients are

$$\epsilon[u]m(a_{yy} - m^2a) + m(\beta - \epsilon[u]_{yy})a - E^{\frac{1}{2}}(b_{yy} - m^2b) = -[u]mF_m h_0 H(y), \tag{6.3a}$$

$$\epsilon[u]m(b_{yy} - m^2b) + m(\beta - \epsilon[u]_{yy})b + E^{\frac{1}{2}}(a_{yy} - m^2a) = 0. \tag{6.3b}$$

From (2.15) we have

$$[u] = U_0 - [\phi(\epsilon\nabla^2\phi + h)_x]/E^{\frac{1}{2}}. \tag{6.4}$$

This can be arranged using (6.1) to obtain

$$[u]^2 = [u]U_0 + [\phi\nabla^2\phi]. \tag{6.5}$$

In terms of a_m and b_m,

$$[u] = U_0 - \tfrac{1}{2}\epsilon\beta\Sigma\frac{m^2(a_m^2 + b_m^2)}{E + \epsilon^2m^2[u]^2} - \tfrac{1}{2}h_0H(y)\Sigma\frac{mF_m}{E + \epsilon^2m^2[u]^2}\{\epsilon m[u]a_m - E^{\frac{1}{2}}b_m\}. \tag{6.6}$$

The system described by (6.3) and (6.6) is closed and could be solved numerically with the side-wall conditions $a_m = b_m = 0$. The effect of including the zonal shear can

be found more easily however. When $H(y) = \sin ly$ the results of §3 suggest parametrizing $[u]$ in terms of U by

$$[u] = U + (U_0 - U)\cos 2ly. \tag{6.7}$$

Analytic results can be obtained when the eddy structure is approximated by

$$a_m = A_m \sin ly, \quad b_m = B_m \sin ly. \tag{6.8}$$

(The system using (6.7) and (6.8) will be referred to as the improved quasi-linear theory.) Collecting coefficients of $\sin ly$ in (6.3) then gives

$$A_m = -mF_m\hat{U}m(\hat{\beta} - \epsilon\hat{U}K^2)/\hat{D}_m, \tag{6.9a}$$

$$B_m = -mF_m\hat{U}E^{\frac{1}{2}}K^2/\hat{D}_m, \tag{6.9b}$$

where
$$\hat{D}_m = EK^4 + m^2(\hat{\beta} - \epsilon\hat{U}K^2)^2,$$

and
$$\hat{U} = U - \tfrac{1}{2}(U_0 - U),$$

$$\hat{\beta} = \beta - 2\epsilon l^2(U_0 - U).$$

Comparing (6.9) with (3.8) shows that U has been replaced by the smaller value $\hat{U}$. This reflects the dcreased advection and topographic generation of eddy vorticity due to the decrease of $[u]$ in mid-channel. Similarly β has been replaced by the approximate potential vorticity gradient $\hat{\beta}$. (Note that the latter modification becomes more important as ϵ increases.)

As in §3 an implicit equation for U can be obtained. We find

$$\frac{U}{U_0} = 1 - \frac{h_0^2}{4}\frac{\hat{U}}{U_0}\Sigma m^2 F_m^2 K^2/\hat{D}_m. \tag{6.10}$$

The same general features of resonance and multiplicity are found as in equation (3.9), but modified as explained below. Further, this result restricts U more closely, to

$$\tfrac{1}{3} < U/U_0 \leqslant 1. \tag{6.11}$$

Solutions to (6.10) can be easily obtained by prescribing everything but h_0, then solving for h_0.

Contours of h_0 for varying ϵ and U, as shown in figure 10, represent graphs of U as a function of ϵ. The topography of figure 2 was used, with $\beta = 0{\cdot}2$. When $E^{\frac{1}{2}} = 0{\cdot}02$ (figure 10*a*) the usual minima appear but no multiple solutions occur. As $E^{\frac{1}{2}}$ is decreased multiple solutions do appear, but in contrast to the simpler theory they fade out as ϵ increases or U decreases (see figure 10*b* with $E^{\frac{1}{2}} = 0{\cdot}01$). With $E^{\frac{1}{2}}$ lowered further to 0·005 (figure 10*c*) the multiplicity becomes more pronounced but the multiple solution regime is little changed.

It is interesting to find a closed loop in figure 10(*c*). This loop cannot be reached simply by varying ϵ slowly as in other multiple branch cases. Presumably some internal fluctuation of a quasi-stationary system is needed to reach such a loop.

The dynamics can still be regarded as a balance of relative advection, dissipation and generation as described in §4, with U and β modified as above. The condition for resonance (no relative advection) is altered to

$$\epsilon\hat{U} = \hat{\beta}/K^2. \tag{6.12}$$

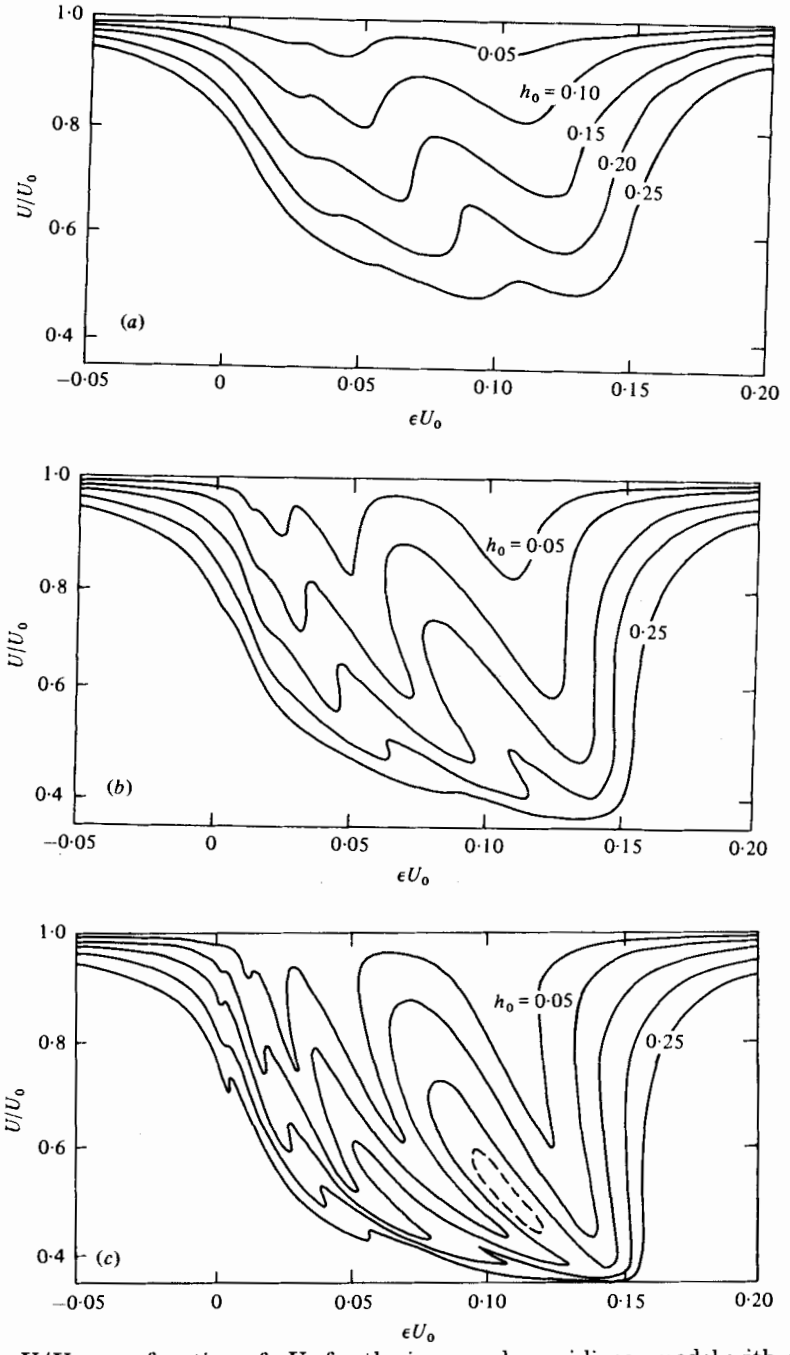

FIGURE 10. U/U_0 as a function of ϵU_0 for the improved quasi-linear model with $\beta = 0{\cdot}2$ and topography height as indicated. (*a*) $E^{\frac{1}{2}} = 0{\cdot}02$, (*b*) $E^{\frac{1}{2}} = 0{\cdot}01$, (*c*) $E^{\frac{1}{2}} = 0{\cdot}005$. The dashed loop is for $h_0 = 0{\cdot}175$. (The other portion of the 0·175 contour is close to the 0·2 contour.)

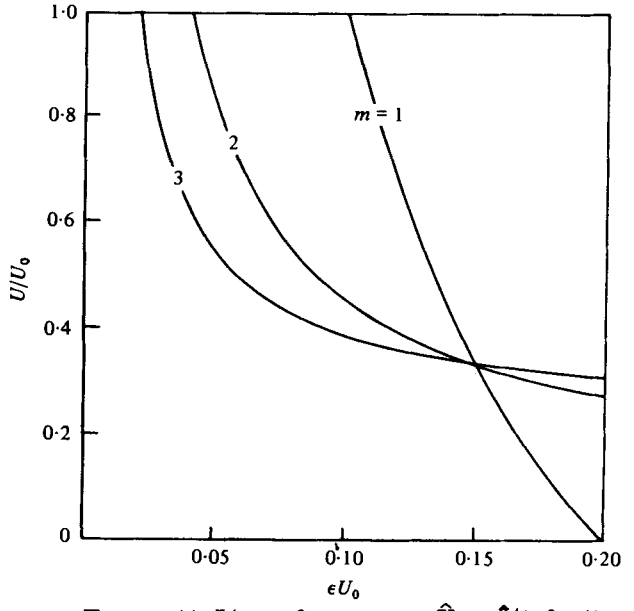

FIGURE 11. Lines of resonance $\epsilon\hat{U} = \beta/(m^2+1)$.

Graphs of (6.12) are given in figure 11 for $\beta = 0{\cdot}2$. For westward flow there is no resonance. For eastward flow the resonance curves in (ϵ, U) space begin at $(\beta/K^2, 1)$. Then U decreases as ϵ increases, and for all K^2 the curves meet at $\epsilon = 3\beta/4l^2$ when $U = \frac{1}{3}$ (the theoretical minimum). This behaviour explains the new bounds on the multiple solution regimes, which rely on the blocked modes that occur near such curves. Approximate boundaries are $\epsilon < 3\beta/4l^2$ and, from (6.12),

$$U > \frac{\beta + \epsilon(K^2/2 - 2l^2)}{\epsilon(3K^2/2 - 2l^2)},$$

where K^2 corresponds to the dominant mode in the topography slope spectrum. (The response is determined by topography slope rather than height when there is a balance of dissipation and generation in a resonant system.)

The improvement gained by the modified theory can be seen in figure 12, where the results are compared with the fully nonlinear numerical model. Very good agreement is found, so the deficits of the simplest theory for relatively large ϵ are due to the neglect of mean shear in the dynamics.

The multiple solutions predicted for $\beta = 0$ by the simplest quasi-linear theory are not found in the improved version. Figure 13 shows the dependence of U/U_0 on ϵU_0 according to (6.10) with $\beta = 0$, and can be contrasted with figure 7. Multiplicity is inhibited by the lower bound on U/U_0.

As an example of the flow patterns predicted by the improved theory, the solutions when $h_0 = 0{\cdot}1$, $E^{\frac{1}{2}} = 0{\cdot}005$, $\beta = 0{\cdot}2$ and $\epsilon = 0{\cdot}14$ are shown in figure 14. The unblocked pattern (figure 14*b*) has $U = 0{\cdot}92$ and is in phase with the topography. The blocked alternative, with $U = 0{\cdot}42$, looks very different with an omega-shaped pattern. (The closed streamline region that appears is not possible in a steady fully nonlinear solution

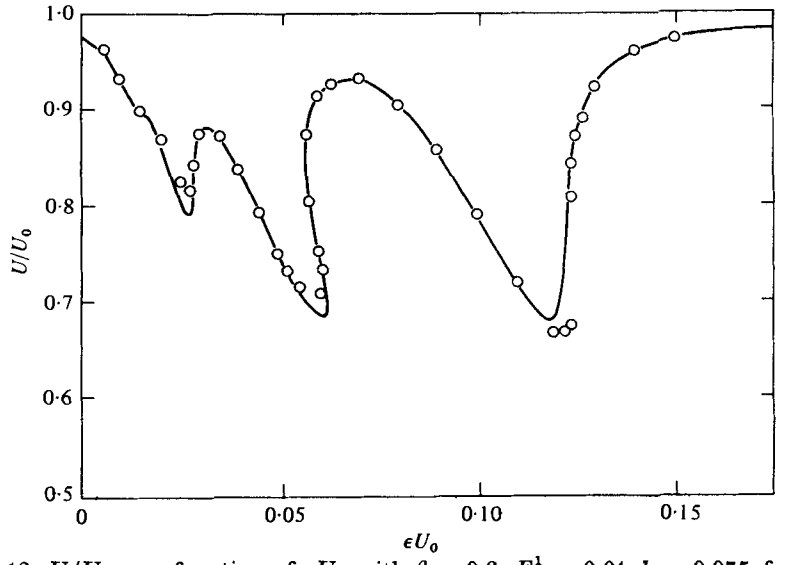

FIGURE 12. U/U_0 as a function of ϵU_0, with $\beta = 0{\cdot}2$, $E^{\frac{1}{2}} = 0{\cdot}01$, $h = 0{\cdot}075$, for the improved quasi-linear (solid line) and fully nonlinear (circles) models.

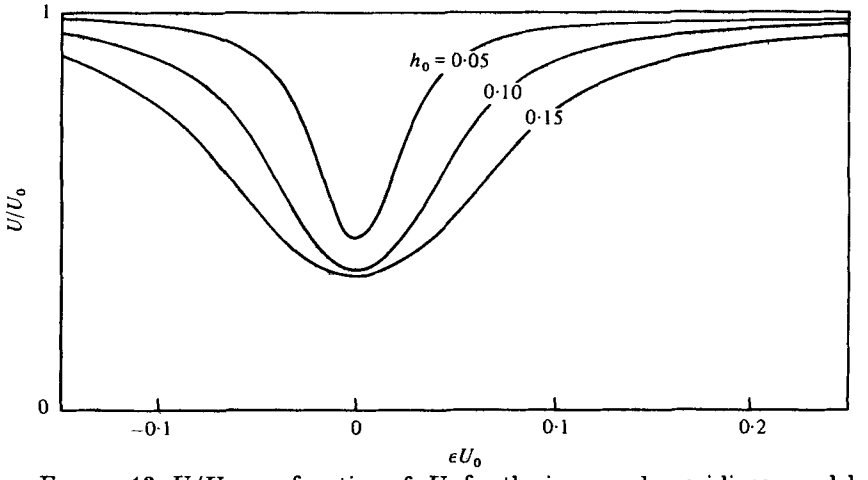

FIGURE 13. U/U_0 as a function of ϵU_0 for the improved quasi-linear model with parameters as in figure 7.

because it violates the circulation condition. However such regions do appear, and persist, in time-dependent systems.)

As well as affecting U and multiplicity, inclusion of mean shear can allow tilting of waves in the flow pattern. Variation of $[u]$ across the channel allows different balances of terms at different latitudes, leading to latitudinal phase changes. This behaviour is evident in figure 15(*a*), which shows streamlines from the fully nonlinear model with $\beta = 0{\cdot}2$, $E^{\frac{1}{2}} = 0{\cdot}01$, $\epsilon = 0{\cdot}03$ and $h_0 = 0{\cdot}2$. The improved quasi-linear theory fixes the eddy structure, however, and allows no wave tilts (see figure 15*b*). (The net mean flow is almost the same though: $U = 0{\cdot}60$ as against $U = 0{\cdot}56$ for the

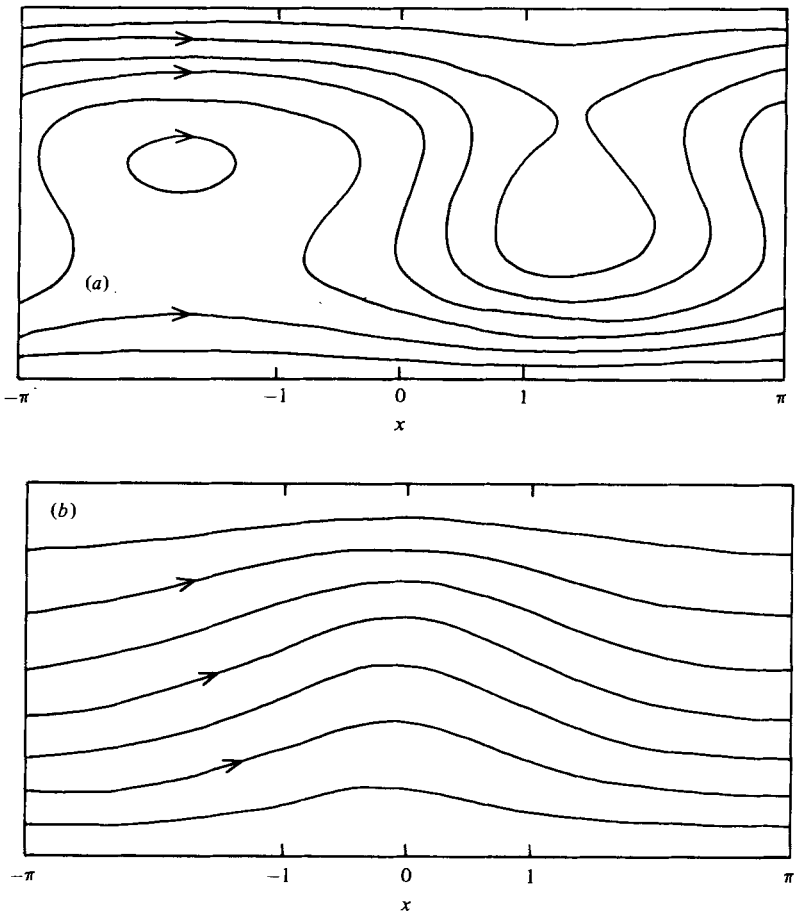

FIGURE 14. Alternative streamlines from the improved quasi-linear model with $\beta = 0{\cdot}2$, $E^{\frac{1}{2}} = 0{\cdot}005$, $h = 0{\cdot}1$, $\epsilon = 0{\cdot}14$. (*a*) $U = 0{\cdot}42$, (*b*) $U = 0{\cdot}92$.

fully nonlinear model.) If the constraint (6.8) is removed and (6.3) solved numerically, with $[u]$ still parametrized as in (6.7), the required wave tilts are obtained (see figure 15*c*).

7. Conclusions

A quasi-linear theory for steady flow over topography in a periodic channel has been developed. The main feature is that feedback between the zonally averaged flow $[u]$ and eddy–topography interactions is allowed. This is an improvement on standard perturbation methods, particularly when Rossby waves are present.

For the simplest model $[u]$ is approximated by a uniform mean flow of unprescribed magnitude. The dynamics can be treated as a balance of eddy-vorticity generation, dissipation and relative advection. It is found that the β-effect reduces the influence of topography for westward flow, and increases it for eastward flow. If dissipation is small Rossby waves can be generated in eastward flow and associated resonance effects appear. Near resonance the flow is very sensitive to the strength of the forcing:

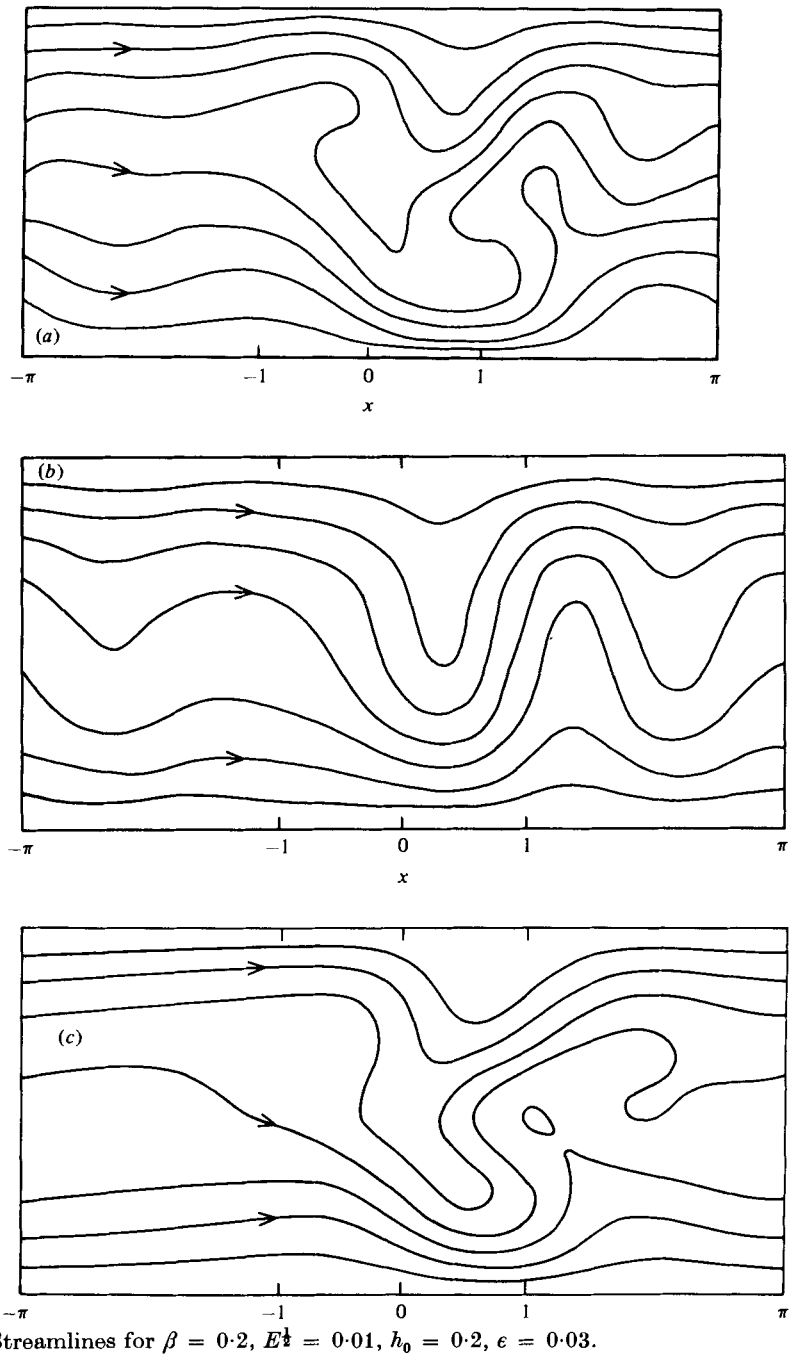

FIGURE 15. Streamlines for $\beta = 0{\cdot}2$, $E^{\frac{1}{2}} = 0{\cdot}01$, $h_0 = 0{\cdot}2$, $\epsilon = 0{\cdot}03$.

(*a*) Fully nonlinear model, $U = 0{\cdot}56$.
(*b*) Improved quasi-linear model, $U = 0{\cdot}60$.
(*c*) Improved model solved numerically, $U = 0{\cdot}56$.

small external changes can cause large changes in the course and magnitude of currents.

Multiple solutions are predicted. Equilibrium curves of U, with varying ϵ, show stable upper and lower branches and an unstable middle branch. As described by Hart (1979) this allows a hysteresis effect as the external forcing varies. The system can switch to a new branch in response to a change in ϵ, then remain on that branch even after ϵ returns to its former value. This has been advanced as a possible explanation for the persistence of blocking patterns in the atmosphere.

A comparison of simplest quasi-linear results with a fully nonlinear numerical model shows good agreement at low ϵ, with predicted multiple solutions confirmed. At larger ϵ however some discrepancies are found. These can be overcome by including mean shear effects. The improved quasi-linear theory, which uses a simple parametrization of $[u]$ in terms of U, gives good analytic results for relatively large as well as low ϵ. It also shows that multiple equilibria are inhibited when mean shear is included.

Results from the analytic and numerical models indicate that the quasi-linear approximation starts to break down when U/U_0 is less than about 0·5. One limiting factor for the steady theory may be barotropic instability. The flow may be unstable if $\beta - \epsilon[u]_{yy}$ reverses sign. For the $[u]$ profile (6.7) this occurs when

$$\epsilon(U_0 - U) > \beta/4l^2. \tag{7.1}$$

This may also be an explanation for oscillations that have been found in some time-dependent fully nonlinear results, and are currently being investigated. (Such behaviour occurs at low $E^{\frac{1}{2}}$ and may represent a transition regime between steady flow and turbulence.)

Another limiting factor is the increasing importance of nonlinear eddy interactions as ϵ increases or $E^{\frac{1}{2}}$ decreases. One way this affects the basic dynamics is as follows. From the exact transport equation (3.3) it can be seen that a low U solution requires a large-amplitude wave of appropriate phase interacting with the topography. Nonlinear effects will tend to transfer energy away from a dominant mode, thus changing U and consequently altering the vorticity balance.

There are several possible extensions of the basic theory. The effects of more general forcing and topography can be added. Time dependence can be included to find the response to fluctuating forcing or background noise, and may be useful for developing a theory for statistically steady systems.

For more specific atmospheric applications on planetary scales spherical geometry should be used, and temperature gradient effects included. Diabatic heating could be added, to study the effect of varying land–sea contrasts for example.

The theory can also be used as a basic model of the Antartic Circumpolar Current (a large ocean current which flows eastward around Antartica and is strongly influenced by topography). On very large scales ($O(10\,000$ km)) advection effects are usually discarded (Smith & Fandry 1978 apply such a theory using two layers and $O(1)$ topography height). Preliminary quasi-linear calculations with stratification suggest that multiple equilibria can occur on such scales. The circumpolar transport may also be influenced by interactions on smaller scales. From an analysis of hydrographic data Gordon & Bye (1972) deduced that stationary Rossby waves with wavelength $O(1000$ km) may occur east of the Campbell Plateau (a large submarine ridge south

of New Zealand). The evidence is inconclusive due to the scarcity of data, but it does suggest that the feedback mechanisms of the quasi-linear theory are important.

Application is not limited to circumpolar geometry. For example, the concept of an implicit basic flow could be used in an idealized model of the North Atlantic circulation to investigate the relation between large gyres and Gulf Stream meanders. Further, Rossby waves with wavelengths up to 200 km have been found on continental rises (see Thompson & Luyten 1976, for example). Interactions of such waves with obstacles (such as canyons) may cause local blocking events, and it is thought that the periodic quasi-linear theory can be modified to study such phenomena.

Most of the work described in this paper was done while at the National Center for for Atmospheric Research, and the support of a post-doctoral fellowship there is gratefully acknowledged. The National Center for Atmospheric Research is sponsored by the National Science Foundation.

Appendix A. An alternative transport equation

The vorticity equation (2.3) is multiplied by p and integrated over the channel to obtain

$$\iint p\{\omega\nabla^2 p_t + E^{\frac{1}{2}}\nabla^2 p - \tfrac{1}{2}E^{\frac{1}{2}}(v_{Tx} - u_{Ty})\}\,dx\,dy = 0. \tag{A 1}$$

(The integral of the Jacobian and β terms vanishes.) Integrating by parts and using periodicity and boundary conditions (2.5) leads to

$$-\iint\left(\tfrac{1}{2}\omega\frac{\partial}{\partial t} + E^{\frac{1}{2}}\right)(u^2+v^2)\,dx\,dy + Q\int\left(\omega\frac{\partial}{\partial t} + E^{\frac{1}{2}}\right)u(x,b)\,dx$$
$$+ \tfrac{1}{2}E^{\frac{1}{2}}\iint(uu_T + vv_T)\,dx\,dy - \tfrac{1}{2}E^{\frac{1}{2}}Q\int u_T(x,b)\,dx = 0. \tag{A 2}$$

The circulation condition (2.8) cancels the side-wall integrals. This leaves the energy equation

$$\left(\tfrac{1}{2}\omega\frac{d}{dt} + E^{\frac{1}{2}}\right)E_k = \tfrac{1}{4}E^{\frac{1}{2}}\iint(uu_T + vv_T)\,dx\,dy, \tag{A 3}$$

where the total kinetic energy of the quasi-geostrophic flow is

$$E_k = \frac{1}{2}\iint(u^2+v^2)\,dx\,dy. \tag{A 4}$$

For the special case $\mathbf{u}_T = (2U_0, 0)$ the right-hand side of (A 3) becomes

$$\tfrac{1}{2}E^{\frac{1}{2}}U_0\iint u\,dy\,dx = E^{\frac{1}{2}}\pi U_0 Q.$$

Thus we have an equation relating Q and E_k:

$$\left(\tfrac{1}{2}\omega\frac{d}{dt} + E^{\frac{1}{2}}\right)E_k = E^{\frac{1}{2}}\pi U_0 Q. \tag{A 5}$$

Appendix B. The standard perturbation method

For perturbations about the basic flow $\mathbf{u} = (U_0, 0)$ we put

$$p = -U_0 y + \delta p_1 + \delta^2 p_2 + \ldots, \tag{B 1}$$

where δ is some expansion parameter. (The choice $\delta = h_0/(E+\epsilon^2)^{\frac{1}{2}}$ as in Davey (1978) gives results valid for the two limits $\epsilon \to 0$ and $E^{\frac{1}{2}} \to 0$, and the range between.) To $O(\delta)$ the vorticity equation gives

$$\epsilon U_0 \delta \nabla^2 p_{1x} + \delta \beta p_{1x} + \delta E^{\frac{1}{2}} \nabla^2 p_1 = -U_0 h_x. \tag{B 2}$$

The steady version of the transport equation (A 5) can be used:

$$Q = \frac{1}{2\pi U_0} \int\int (u^2 + v^2)\, dx\, dy. \tag{B 3}$$

This gives to $O(\delta^2)$

$$\begin{aligned} Q_0 + \delta Q_1 + \delta^2 Q_2 &= \frac{1}{2\pi U_0} \int\int U_0^2 + 2\delta U_0 u_1 + \delta^2 (u_1^2 + v_1^2 + 2U_0 u_2)\, dx\, dy \\ &= Q_0 + 2\delta Q_1 + 2\delta^2 Q_2 + \frac{\delta^2}{2\pi U_0} \int\int (u_1^2 + v_1^2)\, dx\, dy, \end{aligned}$$

where

$$Q_i = \int_0^b u_i\, dy.$$

It follows that

$$Q_1 = 0, \tag{B 4a}$$

$$Q_2 = -\frac{1}{2\pi U_0} \int\int (u_1^2 + v_1^2)\, dx\, dy. \tag{B 4b}$$

There is no change in Q to $O(\delta)$, so (B 2) can be solved with $p_1 = 0$ on $y = 0, b$. Knowing p_1 the transport change Q_2 can be found. The next term p_2 (which includes a mean shear) can then be calculated, and used to find Q_3 etc.

When a Fourier series expansion is used as in § 3 we find

$$\delta^2 Q_2 / Q_0 = -\tfrac{1}{4} h_0^2 \Sigma \frac{m^2 F_m^2 K_i^2}{EK^4 + m^2(\beta - \epsilon U_0 K^2)^2}. \tag{B 5}$$

(Note that the transport change is independent of the choice for δ.) There are two main defects. The transport change is proportional to h_0^2, which is too strong a dependence for changes larger than about 10 %. Second, the response to Rossby-wave resonances is too large and is misplaced.

Appendix C. Spectral equations for the numerical model

Some notation must first be defined. The orthogonal modes for a channel of length 2π and width π are denoted

$$\left.\begin{aligned} c_k &= \sin ny \\ C_k &= \cos mx \sin ny \\ S_k &= \sin mx \sin ny \end{aligned}\right\} \quad \begin{aligned} &\text{for} \quad n = k = 1, \ldots 2N; \\ &\text{for} \quad n = 1, \ldots N, \quad m = 1, \ldots M, \quad k = (m+1)N + n. \end{aligned}$$

Summations to be used are

$$\Sigma = \sum_{1}^{2N}, \quad \Sigma' = \sum_{2N+1}^{2N+MN}.$$

The stream function is written as the truncated series

$$p = -Uy + \Phi + \phi, \tag{C 1}$$

where

$$\Phi = \Sigma a_k(t)\, c_k,$$

$$\phi = \Sigma' A_k(t)\, C_k + B_k(t) S_k.$$

We use topography

$$h = h_0 \Sigma f_k c_k + h_0 \Sigma' F_k C_k + G_k S_k, \tag{C 2}$$

and prescribed upper-surface stream function

$$p_T = -U_T y + \Sigma a_{Tk} c_k + \Sigma' A_{Tk} C_k + B_{Tk} S_k. \tag{C 3}$$

Equations for the spectral coefficients are obtained from the vorticity equation. For the mean shear we find

$$\begin{aligned} 2K_k^2 \omega a_{kt} = {} & 2E^{\frac{1}{2}} K_k^2 (\tfrac{1}{2} a_{Tk} - a_k) - \epsilon \Sigma' \Sigma' K_j^2 (A_i B_j - A_j B_i)\, \alpha_{ijk} \\ & + h_0 \Sigma' \Sigma' (A_i G_j - B_i F_j)\, \alpha_{ijk} \quad (K_k^2 = m^2 + n^2). \end{aligned} \tag{C 4}$$

The eddy/mean-shear interaction coefficient is

$$\alpha_{ijk} = \frac{2}{\pi^2} \int\int J(C_i, S_j) c_k \, dx \, dy.$$

For the eddies,

$$\begin{aligned} \omega K_k^2 A_{kt} = {} & E^{\frac{1}{2}} K_k^2 (\tfrac{1}{2} A_{Tk} - A_k) + (\beta - \epsilon U K_k^2)\, m B_k + U h_0 m G_k \\ & + \sum_i \sum_j{}' (\epsilon K_j^2 B_j - h_0 G_j)\, a_i \alpha_{kji} + \sum_i{}' \sum_j (-\epsilon K_j^2 a_j + h_0 f_j)\, B_i \alpha_{ikj} \\ & + \Sigma' \Sigma' [(-\epsilon K_j^2 B_j + h_0 G_j) A_i \gamma_{ijk}^{(1)} + (-\epsilon K_j^2 A_j + h_0 F_j) B_i \gamma_{ijk}^{(2)}], \end{aligned} \tag{C 5a}$$

$$\begin{aligned} \omega K_k^2 B_{kt} = {} & E^{\frac{1}{2}} K_k^2 (\tfrac{1}{2} B_{Tk} - B_k) - (\beta - \epsilon U K_k^2)\, m A_k - U h_0 m F_k \\ & + \sum_i \sum_j{}' (-\epsilon K_j^2 A_j + h_0 F_j)\, a_i \alpha_{kji} + \sum_i{}' \sum_j (\epsilon K_j^2 a_j - h_0 f_j)\, A_i \alpha_{ikj} \\ & + \Sigma' \Sigma' [(-\epsilon K_j^2 A_j + h_0 F_j) A_i \gamma_{ijk}^{(3)} + (-\epsilon K_j^2 B_j + h_0 G_j) B_j \gamma_{ijk}^{(4)}]. \end{aligned} \tag{C 5b}$$

The eddy–eddy interaction coefficients are

$$\gamma_{ijk}^{(1)} = \frac{2}{\pi^2} \int\int J(C_i, S_j) C_k \, dx \, dy,$$

$$\gamma_{ijk}^{(2)} = \frac{2}{\pi^2} \int\int J(S_i, C_j) C_k \, dx \, dy,$$

$$\gamma_{ijk}^{(3)} = \frac{2}{\pi^2} \int\int J(C_i, C_j) S_k \, dx \, dy,$$

$$\gamma_{ijk}^{(4)} = \frac{2}{\pi^2} \int\int J(S_i, S_j) S_k \, dx \, dy.$$

(There are several symmetries and inter-relations for these coefficients.) The transport equation (2.15) gives

$$\omega U_t = E^{\frac{1}{2}}(\tfrac{1}{2}U_T - U) + \tfrac{1}{4}h_0\Sigma' m(B_k F_k - A_k G_k). \tag{C 6}$$

In the absence of dissipation it can be shown that the total kinetic energy

$$\text{K.E.} = \frac{1}{2}\int\int (u^2+v^2)\,dx\,dy,$$

and the total enstrophy

$$\chi = \int\int (\epsilon\zeta + h + \beta y)^2\,dx\,dy$$

are conserved. (It was found that $2N$ mean-shear modes are required to conserve χ when $\beta \neq 0$.)

Time-stepping from some initial conditions was done using an iterated predictor–corrector scheme. For the results presented in §5, $M = 8$, $N = 4$ was used. (Addition of extra modes produced insignificant changes in results.)

REFERENCES

Charney, J. G. & DeVore, J. G. 1979 Multiple flow equilibria in the atmosphere and blocking. *J. Atmos. Sci.* **36**, 1205–1216.

Charney, J. G. & Eliassen, A. 1949 A numerical method for predicting the perturbations of the middle latitude westerlies. *Tellus* **1**, 38–54.

Clarke, R. A. & Fofonoff, N. P. 1969 Oceanic flow over varying bottom topography. *J. Mar. Res.* **27**, 226–240.

Davey, M. K. 1978 Recycling flow over bottom topography in a rotating annulus. *J. Fluid Mech.* **87**, 497–520.

Egger, J. 1978 Dynamics of blocking highs. *J. Atmos. Sci.* **35**, 1788–1801.

Gordon, A. L. & Bye, J. A. T. 1972 Surface dynamic topography of Antarctic waters. *J. Geophys. Res.* **77**, 5993–5999.

Grose, W. L. & Hoskins, B. J. 1979 On the influence of orography on large-scale atmospheric flow. *J. Atmos. Sci.* **36**, 223–234.

Hart, J. E. 1979 Barotropic geostrophic flow over anisotropic mountains: multiequilibria and bifurcations. *J. Atmos. Sci.* (to appear.)

McIntyre, M. E. 1968 On stationary topography-induced Rossby wave patterns in a barotropic zonal current. *Dt. Hydrogr. Z.* **21**, 203–214.

Manabe, S. & Terpstra, T. B. 1974 The effect of mountains on the general circulation of the atmosphere as identified by numerical experiments. *J. Atmos. Sci.* **31**, 3–42.

Neumann, G. 1960 On the effect of bottom topography on ocean currents. *Dt. Hydrogr. Z.* **13**, 132–141.

Pedlosky, J. 1971 Geophysical fluid dynamics. In *Mathematical Problems in Geophysical Sciences* (ed. W. H. Reid), Lectures in Applied Mathematics vol. 13, pp. 1–60. Providence, Rhode Island: American Mathematical Society.

Smagorinsky, J. 1953 The dynamical influence of large-scale heat sources and sinks on the quasistationary mean motions of the atmosphere. *Quart. J. Roy. Met. Soc.* **79**, 342–366.

Smith, N. R. & Fandry, C. B. 1978 Combined effects of wind stress and topography in a two-layer model of the Southern Ocean. *Deep-Sea Res.* **25**, 371–390.

Thompson, R. O. R. Y. & Luyten, J. R. 1976 Evidence for bottom-trapped topographic Rossby waves from single moorings. *Deep-sea Res.* **23**, 629–635.